

SPACE CHARGE IN IONIZATION DETECTORS AND THE NA48 CALORIMETER*

SANDRO PALESTINI[†]

*CERN, CH-1211 Geneva 23, Switzerland
and INFN - Sezione di Torino, 10125 Torino, Italy
E-mail: sandro.palestini@cern.ch*

The effects of space charge due to slowly drifting ions can be relevant for detectors operated at high intensity, or for relatively low values of the bias voltage. Accurate measurements have been obtained with the liquid krypton calorimeter of the NA48 experiment, from data collected in 1997. The build-up of space charge takes place during the first part of the beam extraction burst, and causes a dependence of the response on the transverse coordinate of the axis of electromagnetic showers, and a small reduction of average amplitude. The effects are well reproduced by a computation, where the only free parameter is the value of the ion mobility. The model can be applied a wide range of operating conditions, and generalized to detectors with different geometry and active medium.

1 Introduction

Ionization detectors are usually not affected by ions, because the induced signal is dominated by the fast drifting electrons, and the total amount of ion charge accumulated in the detector cell is typically much smaller than the charge stored on the electrodes. However, space charge can produce observable effects in case of large particle intensities, or for relatively low values of the bias voltage.

The liquid krypton calorimeter for the NA48 experiment at CERN was operated in 1997 with the bias voltage set at 1.5 kV over a gap of 1 cm, half of the value used in the following years. In this condition, small but precisely measurable effects of space charge have been observed.

In the following sections, after a brief discussion of the design and performance of the NA48 calorimeter, a model of space charge effects in parallel plate detectors is described, and compared to experimental observations. A characteristic, dimensionless parameter is identified, and predictions over wide ranges of operating conditions, cell geometry, and different active media are

*TALK PRESENTED AT CALOR99 – VIII INT. CONF. ON CALORIMETRY IN HEP, LISBON, PORTUGAL, JUNE 13–19,1999

[†]REPRESENTING THE NA48 COLLABORATION: CAGLIARI, CAMBRIDGE, CERN, DUBNA, EDINBURGH, FERRARA, FIRENZE, MAINZ, ORSAY, PERUGIA, PISA, SACLAY, SIEGEN, TORINO, VIENNA, WARSAW

made.

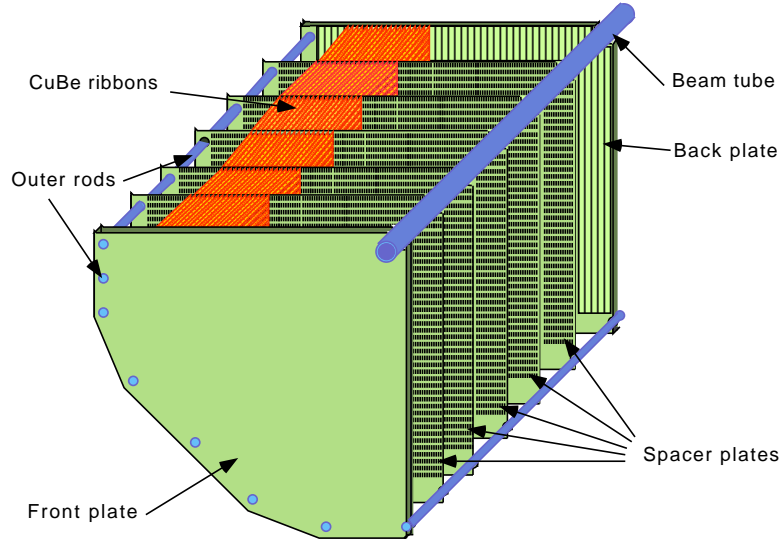


Figure 1. A quadrant of the electrode structure.

2 The NA48 liquid krypton calorimeter

2.1 Detector design

The NA48 electromagnetic calorimeter is a *quasi*-homogeneous device based on liquid krypton.^a Figure 1 sketches the electrode structure. The active surface extends from the beam pipe (8 cm radius) to an octagonal outer boundary 256 cm wide. The read-out cells ($2 \times 2 \text{ cm}^2$) are formed by Cu-Be ribbons, 1.8 cm wide and $40 \mu\text{m}$ thick. The ribbons are stretched between front and back plates made of fiber-glass reinforced epoxy, 127 cm apart, and follow an accordion geometry defined by five thin spacer plates, which guide the electrodes through machined slots at $\pm 48 \text{ mrad}$ from the vertical plane (figure 2). The signals induced on each anode are amplified, shaped to 80 ns

^aLiquid krypton properties: density 2.41 g/cm^3 , radiation length 4.7 cm, Molière radius 4.7 cm, boiling point 119.8 K at 1 atm, electron drift velocity 0.27 (0.33) $\text{cm}/\mu\text{s}$ at 1.5 (3) kV/cm, dielectric constant $\epsilon_R = 1.7$.

FWHM wide signals, and digitized at 40 MHz. For the energy measurement, the sum of the signals from a cluster of about 95 cells is used.

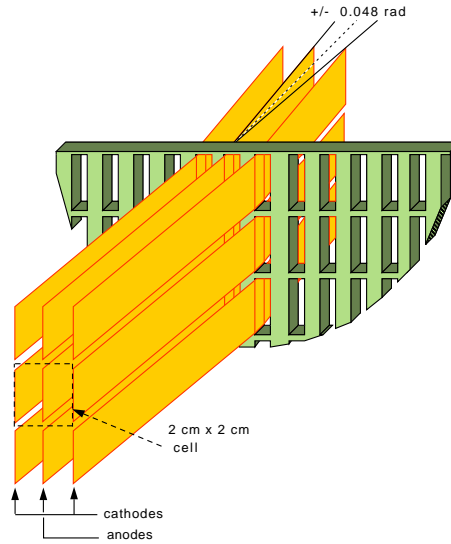


Figure 2. Detail of ribbon electrodes near a spacer plate.

2.2 Detector performance

The performance of the detector has been obtained using electrons from semileptonic kaon decays, for which the momentum P is measured in a magnetic spectrometer, and with special runs taken with electron beams. As shown in figure 3, the energy resolution is $\sigma(E)/E \simeq 0.125/E \oplus 0.032/\sqrt{E} \oplus 0.005$ (E in GeV), where the different terms are added in quadrature. The spatial resolution (figure 3) is better than 1.3 mm and the time resolution is better than 300 ps for showers above 20 GeV.

A discussion of additional detector characteristics particularly relevant for the NA48 physics program can be found in reference 1.

3 Space charge model

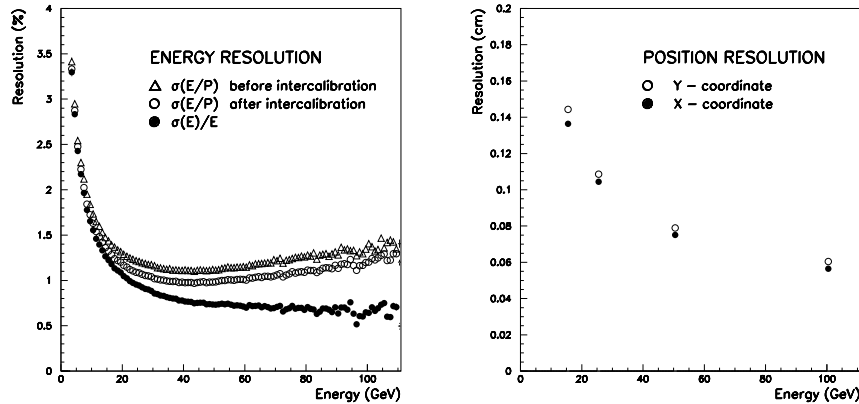


Figure 3. Energy and position resolution as a function of the shower energy. The lowest set of data points in the figure on the left is obtained after unfolding the spectrometer contribution and provides the calorimeter resolution.

3.1 General considerations and assumptions

In order to develop a formalism to describe the effects of space charge, the following observations and assumptions are made:

- the drift velocity of the positive ions is much lower than the electron velocity (v_e), so that only ions effectively contribute to space charge (ρ);
- the ion drift velocity is determined by the mobility coefficient μ , which is assumed constant;
- the ionization detector is approximated as an ideal parallel plate capacitor (with the electric field E along the x direction);
- for the moment, we assume that the injected charge density rate J is uniform inside the cell.

Under the assumptions above, ρ and E must satisfy the charge-conservation equation:

$$\frac{\partial \rho}{\partial t} + \mu E \frac{\partial \rho}{\partial x} + \frac{\mu}{\epsilon} \rho^2 = J \quad (1)$$

where the time evolution of the space charge is related to the the ion drift from anode to cathode (second term), to a term quadratic in ρ (related to

$\partial E/\partial x$, ϵ is the dielectric constant of the medium), and to the charge density injection rate.

3.2 The stationary case

The stationary solution can be written as:

$$\rho = \frac{J x}{\mu E} \quad (2)$$

$$E = \frac{V}{X} \sqrt{C^2 + \alpha^2 \frac{x^2}{X^2}} \quad (3)$$

where V is the value of the bias voltage, X is the width of the cell ($x = 0$ at the anode and $x = X$ at the cathode), C is a numerical integration constant, and the dimensionless parameter α is defined as:

$$\alpha = \frac{X^2}{V} \sqrt{\frac{J}{\epsilon \mu}} \quad (4)$$

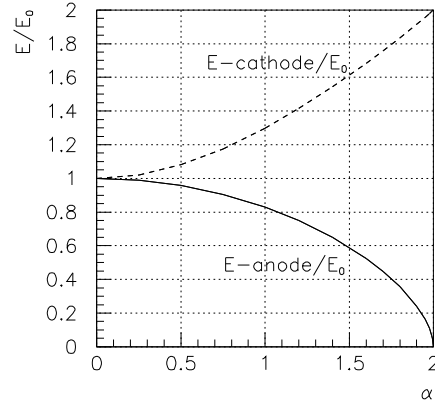


Figure 4. Normalized electric field at anode and cathode vs. α .

The constant C corresponds to the electric field at the anode, divided by $E_0 = V/X$. Figure 4 shows the value of C as function of α , together with the corresponding values of E/E_0 at the cathode. From this and from equation 3, we see that once dimensionless variables x/X , E/E_0 are used, the problem is completely defined by the value of the parameter α . The distortion to the

electric field due space charge can be controlled, with increasing degrees of sensitivity, by changing the values of J , V , and X .^b

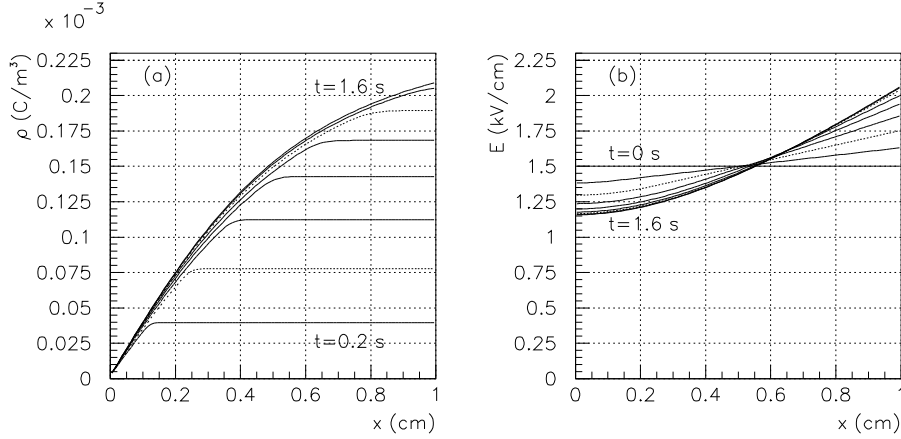


Figure 5. (a) Space charge density and (b) electric field vs. x , for different time values during the charge injection interval, for $\alpha = 1.15$.

3.3 Time dependence

Of particular interest is the case when the charge injection rate J vanishes for $t < 0$, and is constant for $t > 0$. A numerical integration of equation 1 is shown in figure 5, which provides the behavior of ρ and E as functions of x , at various values of t . The following values have been used for the various parameters: $\mu = 0.45 \times 10^{-7} \text{ m}^2 \text{ V}^{-1} \text{ s}^{-1}$, $\epsilon = 1.5 \times 10^{-11} \text{ F m}^{-1}$ (corresponding to liquid krypton), $V = 1500 \text{ V}$, $X = 1.0 \text{ cm}$, and $J = 2.0 \times 10^{-4} \text{ C m}^{-3} \text{ s}^{-1}$ for $t > 0$. The corresponding value for α is 1.15. The different lines for ρ and E correspond to values of t in steps of 0.2 s. The computation shows that a stationary solution is reached for time larger than about 1.5 s, which is equal to the maximum drift time for ions (at low intensity): $X^2/(\mu V)$.

^bModifications are necessary in order to deal with very large space charge density occurring for $\alpha > 2$. A discussion of this, and of some other aspects of space charge effects, can be found in reference 2.

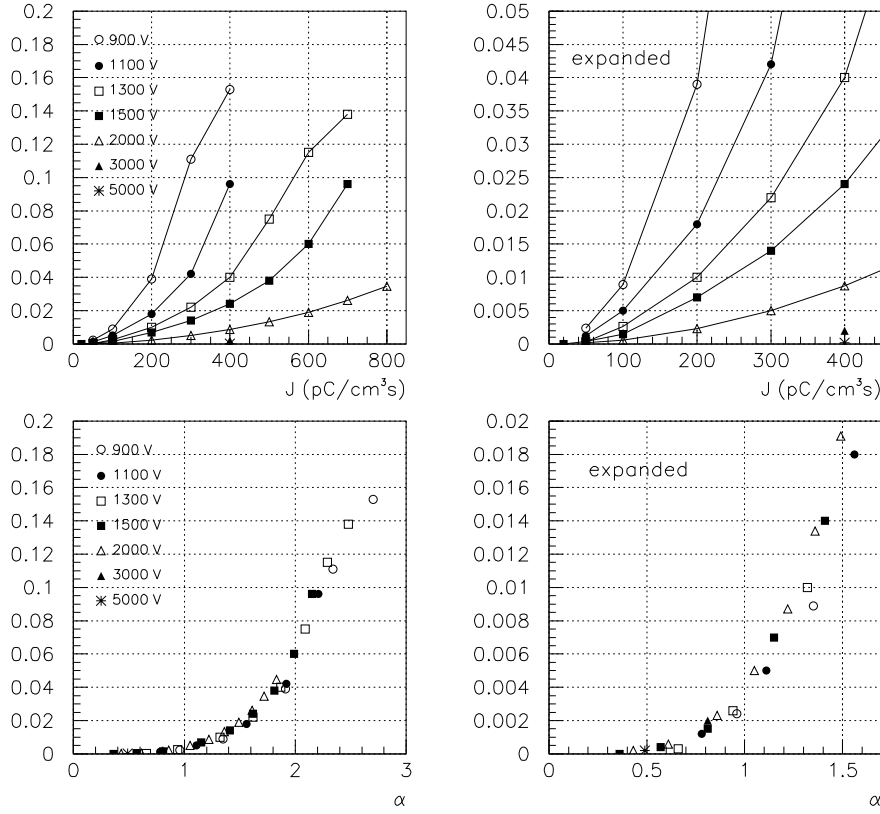


Figure 6. Top: Fractional reduction of average response vs. charge injection rate for liquid krypton, with $X = 1$ and different voltage values. Bottom: as above, but as a function of the parameter α .

4 Ionization detectors

In ionization detectors, the charge deposited at the position x induces on the electrode a current proportional to the electron drift velocity $v_e(x)$, which depends on the local value of the electric field $E(x)$ through the relation between v_e and E . Space charge due to positive ions decreases the response near the anode, and increases it near the cathode, following the trend of $E(x)$. At low intensity ($\alpha \leq 0.5$), the variation in v_e may result to good approximation proportional to the variation in E (i.e.: $\delta v_e/v_e \propto \delta E/E$), and

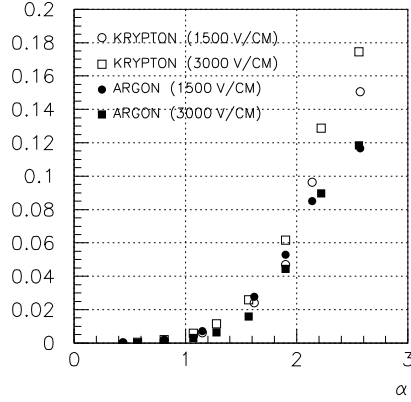


Figure 7. Average reduction of response vs. α on liquid krypton and liquid argon.

the average of the response across the cell width (the *average response*) is unchanged: $\langle v_e \rangle_x = v_e(\langle E \rangle_x) = v_e(E_0)$. For larger values of α the convexity of $v_e(E)$ is such that the increase in v_e near the cathode does not match the decrease at the anode, and the average response of an ionization detector is reduced by the presence of space charge.

Using accurate parametrizations of $v_e(E)$,^{3,4} it is found that to good approximation the reduction in average response depends only on the value of the parameter α , as shown in figure 6 for krypton, and in figure 7 for krypton and argon together.^c We shall refer to this as *approximate scaling* of the reduction of the average response.

A similar situation occurs for calorimeters. The effective charge density injection rate J_{eff} is proportional to the energy flux into the detector, divided by the average ionization energy and by the detector effective depth. The latter depends on the shower longitudinal profile, and for fully absorbed electromagnetic showers, is equal to 13 radiation lengths. Figure 8 shows that approximate scaling is still valid, with the reduction of response depending on $\alpha_{\text{eff}} = \alpha(J_{\text{eff}})$ as in equation 4. The formalism describing the average response is quite general, and can be applied to detectors with different electrode structure, and sampling calorimeters.

^cAs for figure 5, the computations shown in figures 6–8 have been made with the cell width $X = 1$ cm.

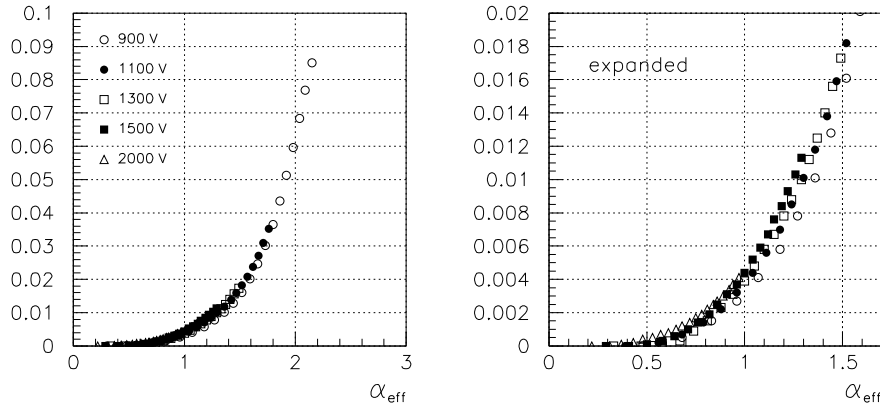


Figure 8. Decrease of average response for showers in krypton, as a function of α .

5 Comparison with measurements

Figure 9(left) shows the reduction in average response, as a function of the time within the beam extraction period, observed with the NA48 calorimeter, operated at 1.5 kV, for showers with radial position $r < 30$ cm. The measurement is performed with electrons from semileptonic kaon decays, comparing the calorimeter energy measurement to the momentum measured in the magnetic spectrometer. The observed trend is compatible with the value $\mu = (0.41 \pm 0.02) \text{ cm}^2 \text{ kV}^{-1} \text{ s}^{-1}$ for the ion mobility. Comparison of response between early showers ($t < 0.1$ s) and late ones ($t > 1.6$ s) provides the *local* variation of response related to $E(x)$, shown in figure 9(right) for showers with $20 < r < 25$ cm.

A comparison between measurements and model predictions can be made based on the mobility value quoted above, and known values for the charge injection rate. Across the NA48 detectors, the particle intensity varied in 1997 from $1500 \text{ GeV cm}^{-2} \text{ s}^{-1}$ at $r = 15$ cm ($\pm 5\%$), to a value 100 times smaller at $r = 120$ cm. The corresponding maximum value for the effective charge injection rate and scaling parameter are $J = 180 \text{ pC cm}^{-3} \text{ s}^{-1}$ and $\alpha_{\text{eff}} = 1.1$.

Figure 10 shows the comparison between data and model predictions. The two lines define the range predicted by the model given the uncertainties in the intensity normalization and in the ion mobility. It should be stressed that the model is not a fit to the data, and its shape and normalization have been obtained from general principles and independent measurements. The

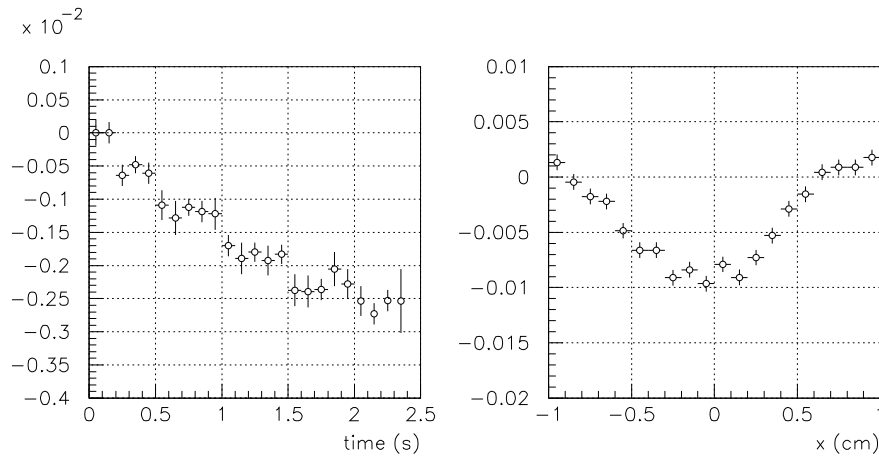


Figure 9. Left: dependence of the average response on the time from the beginning of the extraction period ($r < 30$ cm). Right: dependence of the local response on the shower coordinate within the central read-out cell ($20 < r < 25$ cm). The value $x = 0$ corresponds to the anode, and $x = \pm 1$ to the cathodes.

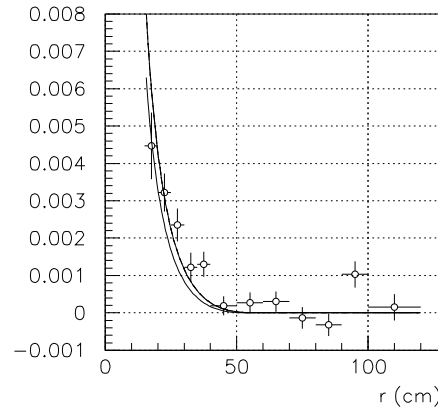


Figure 10. Measured reduction of average response (data points) compared to the model prediction.

good agreement is therefore relevant and establishes confidence in the various assumptions used in this analysis.

Figure 11 shows the peak-to-peak amplitude of the x -dependent (local) non-uniformity of response, as function of the r and of α_{eff}^2 . The latter is

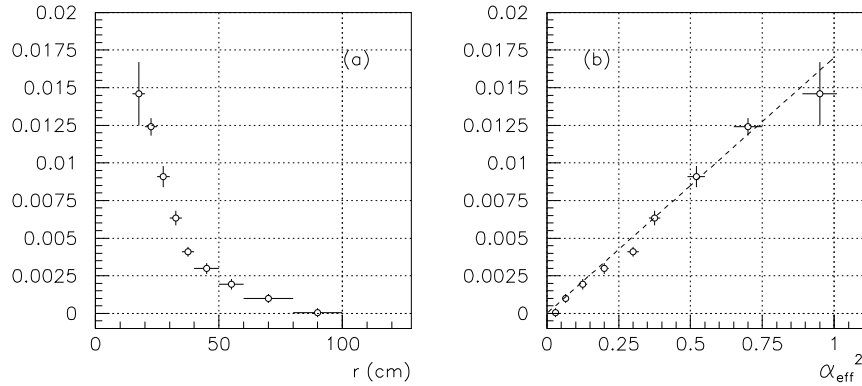


Figure 11. Dependence of the peak-to-peak local modulation of the response on the radial position (a), and on the parameter α_{eff}^2 (b).

characterized by a predictable linear relation.^d

6 Conclusions

Effects caused by space charge due to positive ions have been observed with the liquid krypton calorimeter of the experiment NA48. A model has been developed, characterized by a dimensionless parameter, and suited to describe a wide range of operating conditions and different detector designs. Good agreement is found between experimental data and model predictions.

References

1. V. Fanti et al., preprint CERN-EP/99-114, to appear on *Phys. Lett. B* (1999).
2. S. Palestini et al., *Nucl. Instrum. Methods A* **421**, 75 (1999).
3. A.M. Kalinin, Yu.K. Potrebenikov, A. Gonidec and D. Schinzel, NA48 Note 96-8 (1996).
4. V. Vuillemin et al., *Nucl. Instrum. Methods A* **316**, 71 (1992).

^dThe proportionality coefficient depends on the ratio between cell width and Molière radius, and its value will change for detectors with different read-out cell or medium.